Application of the time-dependent local density approximation to optical activity

K. Yabana*

Graduate School of Science and Technology, Niigata University, Niigata 950-21, Japan

G. F. Bertsch[†]

Physics Department and Institute for Nuclear Theory, University of Washington, Seattle, Washington 98195

As part of a general study of the time-dependent local density approximation (TDLDA), we report here calculations of optical activity of chiral molecules, taking as examples methyloxirane and C_{76}. The theory automatically satisfies sum rules and the Kramers-Kronig relation between circular dichroism and optical rotatory power. It reproduces the absorption strengths of the strong states quite well and qualitatively describes the chiroptical properties; quantitatively, the predictions of the circular dichroism of the lowest states are a factor of 2–4 too high. In the chiral fullerene C_{76} the TDLDA provides a consistent description of the optical absorption spectrum, the circular dichroism spectrum, and the optical rotatory power, except for an overall shift of the theoretical spectrum. [S1050-2947(99)07607-6]

I. INTRODUCTION

The time-dependent local density approximation (TDLDA) as well as the time-dependent Hartree-Fock theory has been applied to the optical absorption of atomic and molecular systems with considerable success [1–14]. Here we want to see how well the TDLDA method does on a more subtle aspect of the optical response, the optical activity of chiral molecules. Calculation of circular dichroism and especially optical rotatory power is more challenging because the operators that must be evaluated are more sensitive to the approximations on the wave function than the electric dipole in the usual form $e\vec{r}$.

The theory can be derived from a variational principle,

$$\delta \int dt \, \langle \Psi | H - i\hbar \frac{\partial}{\partial t} | \Psi \rangle = 0. \tag{1}$$

Here Ψ is restricted to be a Slater determinant of single-electron wave functions ψ_i, $\Psi = \mathcal{A}\Pi_i \psi_i$. The corresponding static variational principle is the usual energy minimization principle from which one derives the Hartree-Fock equations. The Kohn-Sham equations of the LDA theory are obtained in the same way, using the LDA energy functional instead of $\langle \Psi | H | \Psi \rangle$ in Eq. (1). The derived TDLDA equations of motion are given by

$$-\frac{\hbar^2 \nabla^2}{2m} \psi_i + V_{\text{ion}}\psi_i + e^2 \int dr' \frac{n(r')}{|r-r|} \psi_i + V_{\text{xc}}[n(r)]\psi_i$$

$$= i\hbar \frac{\partial}{\partial t}\psi_i, \tag{2}$$

where $n(r) = \Sigma_i |\psi_i(r)|^2$ is the electron density. The V_{xc} is the exchange-correlation potential, related to the exchange-correlation energy v_{xc} by $V_{\text{ex}} = dv_{\text{xc}}/dn$.

Several general remarks can be made here. Practitioners of the density-functional theory often claim justification for the Kohn-Sham equations based on formal existence theorems. Theorems can also be proven for the time-dependent case [15], but our own partiality to the theory is based on more pragmatic considerations. First, if the time dependence is slow, the TDLDA should be as good as the static theory because the motion would be adiabatic and governed by the same Hamiltonian. Second, integrals of the response over frequency obey sum rules, and these are satisfied in principle by the small-amplitude TDLDA. Since the sum rules are most sensitive to the high frequency behavior, we see that the TDLDA is good at both extremes, and therefore promising for describing the middle ground.

There are of course intrinsic limitations in the TDLDA theory. It describes the system by a single Slater determinant which can be expressed in a particle-hole basis as a particle-hole operator on the ground state. We thus do not expect it to be useful for strongly correlated systems, which do not have a single Slater determinant dominating the wave function. Even if the ground state is well described by a single configuration, the description of the excitation by a single Slater determinant does not contain the degrees of freedom necessary to describe excitations that have a more complex character than single-electron excitations. Not only will the experimental spectrum be more complex due to mixing of states of different particle-hole character, but the coupling to vibrations will broaden the transitions on an energy resolution scale of a few tenths of an eV. However, even though the TDLDA only includes single-electron degrees of freedom, it is far superior to the static single-electron theory because it includes dynamic screening effects. The dynamic screening arises directly from the time dependence of the mean field potential. It shifts transition strength up out of the lowest particle-hole excitations into a higher frequency range, of course preserving the sum rule. This can be a very large effect; in the case of C_{76} considered below, the strength of the lowest excitations is reduced by an order of magnitude.

*Electronic address: yabana@nt.sc.niigata-u.ac.jp

[†]Electronic address: bertsch@phys.washington.edu

While the TDLDA has been proved useful for describing the electric dipolar response, its effectiveness dealing with the magnetic response has not been as well explored. The TDLDA is derived by optimizing a wave-function constructed from (time-dependent) single-particle wave functions, so its domain of validity should be all one-particle observables, including the magnetic current operator. We use a wave-function language, but the actual object of the theory is the single-particle density matrix $n(r,r')$.

In our implementation of TDLDA [8], we represent the electron wave function on a uniform spatial grid. The real-time evolution of the wave function is directly calculated and the response functions are calculated by the time-frequency Fourier transformation. The method respects sum rules and the Kramers-Kronig relation between the circular dichroism and optical rotatory power. Since the grid representation is bias-free with respect to electromagnetic gauge, it is not subject to the gauge difficulties encountered when the space of the wave function is constructed from an atomic orbital representation.

Optical activity has been a challenging problem for computational chemistry, but there has been considerable progress in recent years. For example, Carnell *et al.* [16] present a good description of the circular dichroism of excited states of *R*-methyloxirane using a standard Gaussian representation of the wave function. The optical rotatory power is a much more difficult observable, since the whole spectrum contributes. Only very recently have *ab initio* calculations been reported for this property [17,18].

After presenting our calculational method, we report our exploratory study on optical activities of two chiral molecules: *R*-methyloxirane, a simple 10-atom molecule with known chiroptical properties up to the first few excited states [16,19,20], and C_{76}, a fullerene with very large optical rotatory power and significant circular dichroism in the visible and uv [21].

II. FORMALISM

A. Some definitions

Polarization of a chiral molecule in an applied electromagnetic field is expressed using two coefficients α and β as [22]

$$\vec{p} = \alpha\vec{E} - \frac{\beta}{c}\frac{\partial\vec{B}}{\partial t}. \tag{3}$$

Here α is the usual polarizability and is given microscopically as

$$\alpha(E) = e^2\sum_n \left(\frac{1}{E_{n0}-E-i\delta} + \frac{1}{E_{n0}+E+i\delta}\right) \times \frac{1}{3}\langle\Phi_0|\sum_i \vec{r}_i|\Phi_n\rangle^2, \tag{4}$$

where Φ_n and E_n are the eigenvector and eigenvalue of the nth eigenstate of the many-body Hamiltonian H, $H\Phi_n = E_n\Phi_n$, and $E_{n0}=E_n-E_0$. The δ is an infinitesimal positive quantity. Employing the oscillator strength

$$f_n = \frac{2mE_{n0}}{\hbar^2}\frac{1}{3}\langle\Phi_0|\sum_i \vec{r}_i|\Phi_n\rangle^2, \tag{5}$$

we define the optical absorption strength whose integral is normalized to the active electron number,

$$S(E) = \sum_n \delta(E-E_{n0})f_n. \tag{6}$$

It is related to the imaginary part of the polarizability,

$$S(E) = \frac{2mE}{\hbar^2e^2}\frac{\text{Im }\alpha(E)}{\pi}. \tag{7}$$

The basic quantity which characterizes the chiroptical transition is the rotational strength defined by [23]

$$R_n = -\frac{e^2\hbar}{2mc}\langle\Phi_0|\sum_i \vec{r}_i|\Phi_n\rangle\cdot\langle\Phi_n|\sum_i \vec{r}\times\vec{\nabla}|\Phi_0\rangle. \tag{8}$$

We define the complex rotational strength function,

$$\mathcal{R}(E) = \sum_n \left(\frac{1}{E_{n0}-E-i\delta} - \frac{1}{E_{n0}+E+i\delta}\right)R_n. \tag{9}$$

The β function in Eq. (3) is related to $\mathcal{R}(E)$ by $\beta(E) = (\hbar c/3E)\mathcal{R}(E)$. We will also use the rotational strength function $R(E)$ defined by

$$R(E) = \sum_n \delta(E-E_{n0})R_n = \frac{\text{Im }\mathcal{R}(E)}{\pi}. \tag{10}$$

As is seen below, the optical rotatory power is proportional to the real part of $\beta(E)$, and the circular dichroism to $R(E)$. They are related to each other by Moscowitz's generalized Kramers-Kronig relation [24].

The difference of the complex indices of refraction for left and right circularly polarized light is proportional to $\mathcal{R}$ in dilute media; the relation is

$$n_L - n_R = \frac{8\pi N_1}{3}\mathcal{R}(E), \tag{11}$$

where N_1 is the number of molecules per unit volume. For comparison with experiment, the common measure of circular dichroism is the decadic extinction coefficient, given by

$$\Delta\epsilon = \frac{4\pi}{\lambda_{\text{cm}}C\log_e 10}\text{Im}(n_L - n_R), \tag{12}$$

where C is the concentration of molecules in moles/liter and the subscript on the wavelength λ is a reminder to express it in centimeters. The optical rotatory power is conventionally reported as

$$[\alpha] = 180°\frac{10}{C_{\text{gm}}\lambda_{\text{cm}}}\text{Re}(n_L - n_R), \tag{13}$$

where C_{gm} is the concentration of molecules in gm/cm^3.

B. Real-time TDLDA

We first rewrite the above strength functions as time integrations. We employ the time-dependent wave function $\Psi(t) = \exp[-iHt/\hbar]\Psi(0)$ with the initial wave function at $t = 0$ given by $\Psi(0) = \exp[ik\Sigma_i z_i]\Phi_0$, where k is a small wave number. In the linear response, the time-dependent polarizability is proportional to the dipole matrix element, $z(t) = \langle \Psi(t)|\Sigma_i z_i|\Psi(t)\rangle$. The frequency-dependent polarizability in the z direction is then obtained as the time-frequency Fourier transformation of $z(t)$,

$$\alpha_z(E) = \frac{e^2}{k}\int_0^\infty \frac{dt}{\hbar} e^{i(E+i\delta)t/\hbar} z(t). \quad (14)$$

The polarizability $\alpha(E)$ is given by the orientational average, $\alpha = (\alpha_x + \alpha_y + \alpha_z)/3$.

Similarly, we denote the angular momentum expectation value as $L_z(t) = \langle \Psi(t)|-i(\vec{r}\times\nabla)_z|\Psi(t)\rangle$. To linear order in k, we may express it as

$$L_z(t) = -2k\sum_n \cos\left(\frac{E_{n0}t}{\hbar}\right)\langle \Phi_0|\sum_i z_i|\Phi_n\rangle$$

$$\times \langle \Phi_n|\sum_i (\vec{r}_i\times\vec{\nabla}_i)_z|\Phi_0\rangle. \quad (15)$$

The complex rotatory strength function $\mathcal{R}(E)$ is expressed as

$$\mathcal{R}_z(E) = \frac{e^2\hbar}{2mc}\frac{i}{k}\int_0^\infty \frac{dt}{\hbar} e^{(E+i\delta)t/\hbar} L_z(t)$$

$$= \frac{e^2\hbar}{2mc}\sum_n \left(\frac{1}{E_{n0}-E-i\delta} - \frac{1}{E_{n0}+E+i\delta}\right)$$

$$\times \langle \Phi_0|\sum_i z_i|\Phi_n\rangle\langle \Phi_n|\sum_i (\vec{r}\times\vec{\nabla})_z|\Phi_0\rangle. \quad (16)$$

$\mathcal{R}(E)$ of Eq. (9) is the sum over three directions, $\mathcal{R} = \mathcal{R}_x + \mathcal{R}_y + \mathcal{R}_z$.

To apply the TDLDA, we prepare the initial single electron orbitals as $\psi_i(0) = \exp[ikz]\phi_i$, where ϕ_i is the static Kohn-Sham orbitals in the ground state. The $\psi_i(t)$ is obtained by intgrating the time-dependent equation, Eq. (2). $n(\vec{r},t) = \Sigma_i|\psi(\vec{r},t)|^2$. The time-dependent dipole moment may be evaluated as $z(t) = \Sigma_i\langle\psi_i|z|\psi_i\rangle$ and the similar expression for $L_z(t)$. The strength functions are then evaluated with Eqs. (14) and (16).

C. Sum rules

According to the TRK sum rule, the integral of $S(E)$ is equal to the number of active electrons N. This sum rule is respected by the TDLDA. It also appears in the short time behavior of $z(t)$ as

$$z(t) = N\frac{\hbar k}{m}t \quad (t \text{ small}). \quad (17)$$

For the rotational strength, we define energy-weighted sums as

$$R^{(n)} = \int_0^\infty dE\, E^n R(E). \quad (18)$$

It is known that $R^{(n)}$ for $n \le 4$ vanishes identically in the exact dynamics [23,25–27]. The vanishing of $R^{(0)}$ in the time-dependent Hartree-Fock theory was first noticed in [28]. The short time behavior of $L(t) = L_x(t) + L_y(t) + L_z(t)$ is related to $R^{(n)}$ as

$$\frac{e^2\hbar}{2mc}L(t) = 2k\left\{R^{(0)} - \frac{R^{(2)}}{2!}\left(\frac{t}{\hbar}\right)^2 + \frac{R^{(4)}}{4!}\left(\frac{t}{\hbar}\right)^4\right.$$

$$\left. -\frac{R^{(6)}}{6!}\left(\frac{t}{\hbar}\right)^6 + \cdots\right\}. \quad (19)$$

Here we note that $L(t)$ is an even function of t as seen in Eq. (15). Since $R^{(n)} = 0$ for $n \le 4$, we see that $L(t)$ behaves as t^6 for small time. $L_i(t)$ $(i = x,y,z)$ behave as t^2 at small t and the cancelation up to t^4 order occurs after summing up three directions. In the TDLDA dynamics, we confirmed that at least t^0 and t^2 coefficients of $L(t)$, namely $R^{(0)}$ and $R^{(2)}$, vanish identically.

D. Numerical details

The TDLDA uses the same Kohn-Sham Hamiltonian as is used in ordinary static LDA calculations. As is common in condensed matter theory, we use pseudopotentials that include the effects of K-shell electrons rather than these electrons explicitly. The pseudopotentials are calculated by the prescriptions of Refs. [29] and [30]. We employ the simple exchange-correlation term proposed in Refs. [31,32]. There are improved terms now in use [34,33], but it was not deemed important for our application.

There are many numerical methods to solve the equations of TDLDA. Ours uses a Cartesian coordinate space mesh to represent the electron wave functions [35], and the time evolution is calculated directly [8,9,36]. There are only four important numerical parameters in this approach: the mesh spacing, the number of mesh points, the time step in the time integration algorithm, and the total length of time that is integrated. We have previously found that the carbon molecules can be well treated using a mesh spacing of 0.3 Å [9,36]. We find that 0.25 Å is necessary for methyloxirane to represent accurately the orbitals around oxygen. We take the spatial volume to be a sphere of radius 8 Å both for methyloxirane and C_{76} presented below. The total number of mesh points, defining the size of the vector space, is about $4\pi R^3/(3\Delta x^3) \sim 80\,000$ $(140\,000)$ for a mesh size of 0.3 Å (0.25 Å).

The algorithm for the time evolution is quite stable as long as the time step Δt satisfies $\Delta t < \hbar/|H|$, where $|H|$ is the maximum eigenvalue of the Hamiltonian. This is mainly dependent on the mesh size. For $\Delta x = 0.3$ Å, we find that $\Delta t = 0.002\hbar/\text{eV}$ is adequate. We integrate the equation of motion for a length of time $T = 60\hbar/\text{eV}$ for C_{76} ($50\hbar/\text{eV}$ for methyloxirane). Then individual states can be resolved if their energy separation satisfies $\Delta E > 2\pi\hbar/T \sim 0.1$ eV.

Our numerical implementation, namely a grid representation of the wave function and the time-frequency Fourier transformation for the response calculation, has several ad-
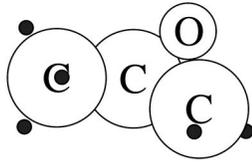
FIG. 1. View of R-methyloxirane with hydrogen on the chiral carbon in the back (and not seen). The chirality is R because the three other bonds are arranged clockwise in the sequence: O, CH_3, and CH_2.

vantages over the usual approach using basis functions centered at the ions. They include the following.

(i) The full spectrum of the wide energy region may be calculated at once and it respects sum rules. The nonlocality of the pseudopotential may cause a violation of the sum rule, but the effect is small in the present systems.

(ii) Since the circular dichroism $R(E)$ and the optical rotatory power, real part of $\beta(E)$, are calculated as a Fourier transformation of the single function $L(t)$, the Kramers-Kronig relation is automatically satisfied.

(iii) The gauge independence of the results is satisfied to high accuracy. Employing the commutation relation $[H, \Sigma_i \vec{r}_i] = -\hbar^2/m \Sigma_i \vec{\nabla}_i$, there are alternative expressions for optical transitions with a gradient operator instead of a coordinate. For the rotational strength, for example,

$$R_n = -\frac{e^2 \hbar^3}{2m^2 c E_{n0}} \langle \Phi_0 | \sum_i \vec{\nabla}_i | \Phi_n \rangle \langle \Phi_n | \sum_i \vec{r}_i \times \vec{\nabla}_i | \Phi_0 \rangle. \tag{20}$$

The strength function with this expression may be calculable with an initial wave function $\psi_i(0) = \exp[id\nabla_z]\phi_i$ with small displacement parameter d. Since the grid representation of the wave function does not have any preference for the gauge condition, our method gives almost identical results for the coordinate and gradient expressions of dipole matrix elements.

III. R-METHYLOXIRANE

The geometry of R-methyloxirane is shown in Fig. 1. We use the same nuclear distances as in Ref. [16]. We show in Fig. 2 the results of the static calculation for the orbital energies. We find a lowest unoccupied molecular orbital (LUMO) 6.0 eV above the highest occupied molecular orbital (HOMO), and a triplet of unoccupied states 0.5 eV higher. In our calculation the lowest unoccupied orbitals have a diffuse, Rydberg-like character, s wave for the lower and p wave for the upper, as in previous calculations [16,37]. The HOMO is localized in the vicinity of the oxygen atom, and the measured absorption strength seen at 7.1 and 7.7 eV is attributed to the excitation of a HOMO electron to the diffuse states. In the TDLDA, the excitation energy comes out close to the orbital difference energies, except for strongly collective states. Indeed we find in the TDLDA calculation that the excitations are within 0.1 eV of the HOMO-LUMO energy and the energy difference for the next state above the LUMO. This is 1 eV less than the experimental values. It is known that the LDA energy functional that we use is subject to overbinding excitations close to the ioniza-
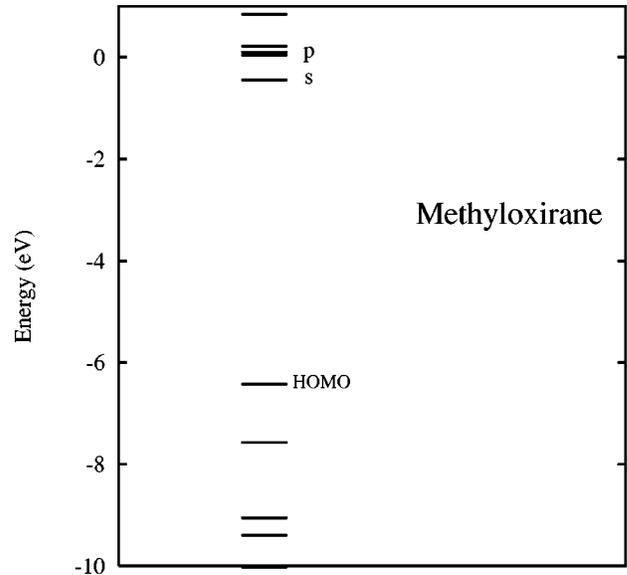

FIG. 2. Static LDA orbitals in methyloxirane.

tion threshold. There are improved energy functions that rectify this problem [38], but for this work we judged the error not important.

The next property we examine is related to the electric dipole matrix element, namely the oscillator strength f associated with the transition. The optical absorption strength is shown in Fig. 3. The total strength up to 100 eV excitation is $f = 22.4$, which is 93% of the sum rule for the 24 active electrons. Notice the lowest two peaks, centered at 6.0 and 6.5 eV. These are the states in which we are interested. Their oscillator strengths are given in Table I. We see that the states are both weak, less than a tenth of a unit. The effect of the time-dependent treatment is to lower the strengths by 30–50 %. This is the well-known screening effect associated with virtual transitions of more deeply bound orbitals. We find that the computed transition strengths are within a factor of 2 of the measured ones. Typically, the TDLDA does somewhat better than this, but most of the experience has
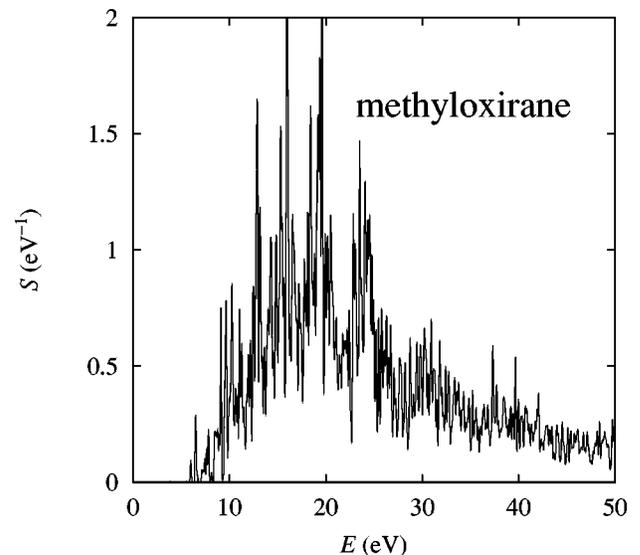

FIG. 3. Optical absorption strength of methyloxirane in the energy region 0–50 eV.

TABLE I. Transitions in R-methyloxirane.

Level		TDLDA	LDA (free)	Other theory		Experiment	
				Ref. [16]	Ref. [19]	Ref. [16]	Ref. [19]
1	E (eV)	6.0	5.97	6.25(7.12)	6.40	7.07	7.12
	f	0.012	0.021		0.0004[a]		0.025
	R ($\times 10^{40}$ cgs)	-23.0	-10.4	-6.43	-2.66[a,b]	-12.56	-11.8[b]
2-4	$\bar{E}$ (eV)	6.5	6.55	6.95	7.3	7.70	7.75
	Σf	0.044	0.069		0.0012[a]		0.062
	ΣR ($\times 10^{40}$ cgs)	23.0	29.9	7.93	2.24[a,b]	6.98	10.8[b]

[a]Calculation with coordinate expression of dipole moment.
[b]Negative of value for S-methyloxirane.

been with transitions carrying at least a tenth of a unit of oscillator strength. The original theoretical calculation gave very poor transition strengths [19], off by more than an order of magnitude. Unfortunately, the more recent study [16] did not include theoretical transition strengths.

We numerically confirmed that our method gives almost identical results with coordinate and gradient expressions of dipole matrix elements, as we remarked in the preceding section. However, exceptionally, the oscillator strength of the very weak features discussed above suffers substantial dependence on the expression. With a gradient formula for the transition matrix elements, strengths of both first and second transitions are larger by about a factor 2 than the coordinate expression. Since the gradient formula emphasizes high-momentum components more heavily, we think the results with coordinate matrix elements may be more reliable for low transitions, and we quote them in Table I.

We now turn to the chiroptical response. Figure 4 shows the short-time behavior of $L_x(t)$ and the sum of the three Cartesian components $L(t) = \Sigma_i L_i(t)$. An initial perturbation of $k = 0.001$ Å^{-1} is employed. To within numerical precision, $L_x(t)$ (solid line) grows with time as t^2, as discussed below Eq. (20). The same is true for the other two components, L_y and L_z. This shows that the numerical algorithm

respects the first sum rule. The combined response $L(t)$ (dashed lines) shows an extreme cancelation at short times, as required by the additional sum rules. However, our numerical accuracy does not allow us to determine the order of the power behavior. The evolution of $L(t)$ for larger times is shown in Fig. 5. Physically, the TDLDA breaks down at long times because of coupling to other degrees of freedom. A typical width associated with such couplings is of the order of a tenth of an eV, implying that the responses damp out on a time scale of $T \approx 10\hbar/\text{eV}$. We note that the TDLDA algorithm itself is very stable, and allows us to integrate to much larger times and obtain very sharp theoretical spectra.

We next show the Fourier transform of the chiroptical response. The circular dichroism spectrum calculated with Eq. (16) is shown in Fig. 6. Here we have integrated L to $T = 50\hbar/\text{eV}$, including a filter function in the integration to smooth the peaks. One can see that the s and the p transitions are clearly resolved, although the three p transitions are not resolved from each other (as is the experimental case). The s transition has a negative circular dichroism and the p transition a positive one. Integrating over the peaks, the strengths of the two peaks are -0.0014 and $+0.0014$ Å^3 eV, respectively. The strengths are commonly quoted in cgs units; the conversion factor is 1 eV Å$^3 = 1.609 \times 10^{-36}$ erg cm^3. The
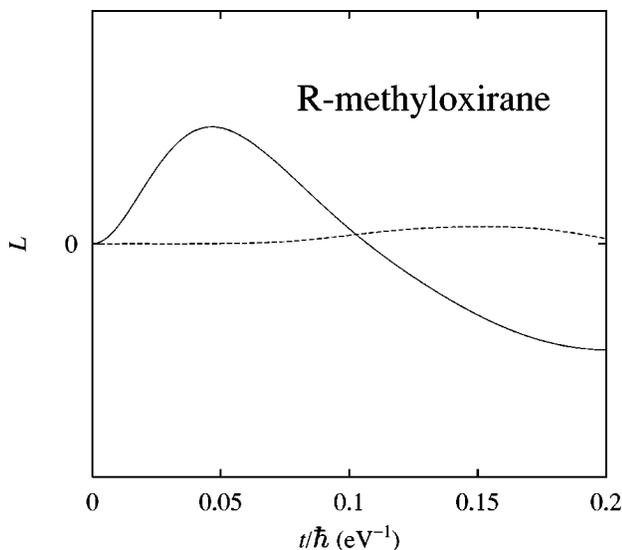

FIG. 4. Short-time chiroptical response of R-methyloxirane. The solid line is $L_x(t)$, dashed line is $\Sigma_i L_i(t)$.
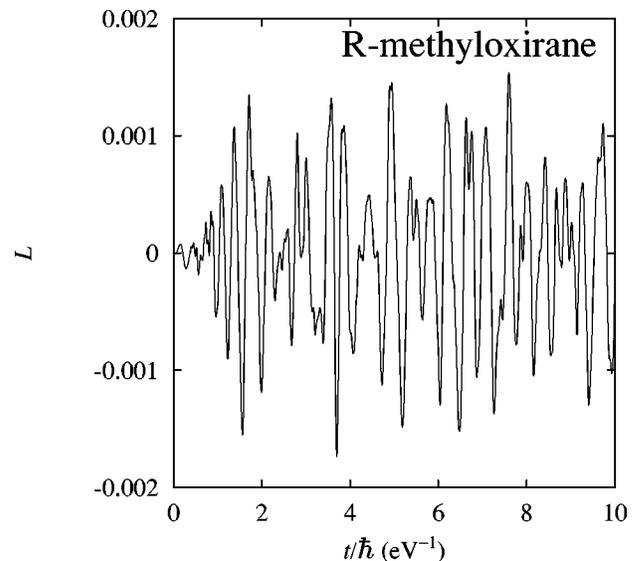

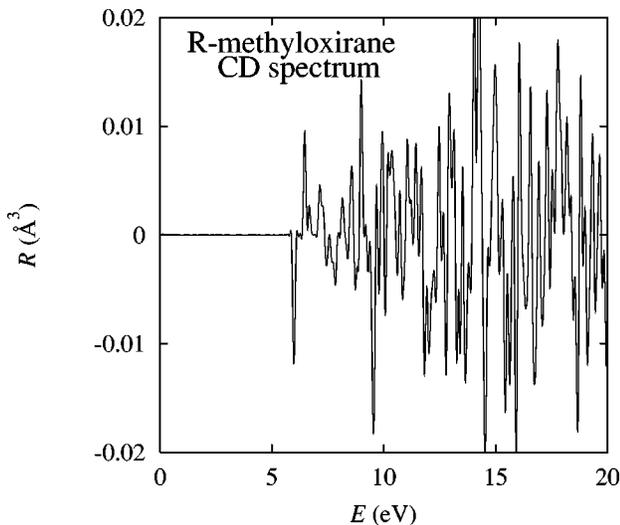FIG. 5. Chiroptical response of R-methyloxirane $L(t)$ for longer times.

FIG. 6. R in R-methyloxirane in the interval 0–20 eV.

FIG. 7. Optical rotatory power Re β at $E = 2.1$ eV as a function of cutoff energy E_{max} in the integration of Eq. (22).

values in cgs units are given in Table I, compared to experiment and previous calculations. We find the signs are correctly given, but the values are somewhat too high, by a factor of 2 or 3. The calculation of Ref. [16] gave a result within the experimental range for the p multiplet but too small (by a factor of 2) for the s transition. Thus we find that the TDLDA has a somewhat poorer accuracy in this case.

Next we consider the optical rotatory power. It could be calculated as the real part of the Fourier transformation Eq. (16). In practice, however, we found that the calculation employing the Kramers-Kronig relation to the rotational strength function,

$$\mathrm{Re}\,\beta(E) = \frac{2}{3}\hbar c \int_0^\infty dE' \frac{R(E')}{E'^2 - E^2}, \qquad (21)$$

gives a more accurate result, especially at the energy below the lowest transition. The measurement is available at the sodium D line, 2.1 eV, $[\alpha]_D = +14.65°$ [37], which gives $\beta = +0.0017$ Å^4. The calculated value at low energy is very sensitive to the number of states included in the sum. Figure 7 shows the calculated value as a function of a cutoff energy, upper bound in the integration in Eq. (22). The value taking only the contribution of the lowest transition is -0.06. Including more states produces values that fluctuate in sign and magnitude within that range. Including all states below 100 eV gives a cancelation by a factor of 60 to yield a value $\beta = -0.001$ Å^4. This has the opposite sign but the same order of magnitude as the measured β. Clearly, to get high relative accuracy with such a strong cancelation is more demanding than our TDLDA can provide.

IV. C$_{76}$

Remarkably, it is possible to separate the chiral partners of the double-helical fullerene C$_{76}$ using stereospecific chemistry [21]. The molecule shows a huge optical rotatory power, $[\alpha]_D = -4000°$, and a complex circular dichroism spectrum between 2 and 4 eV excitation [21]. There has been reported only a semiempirical quantum chemistry calculation for the optical activity of this molecule [39].
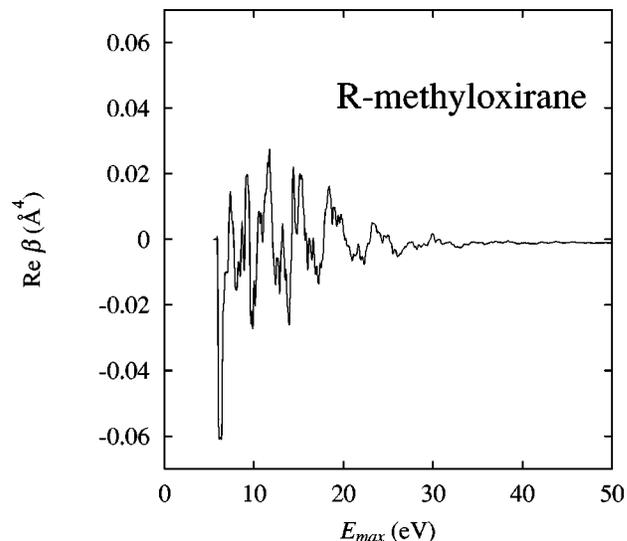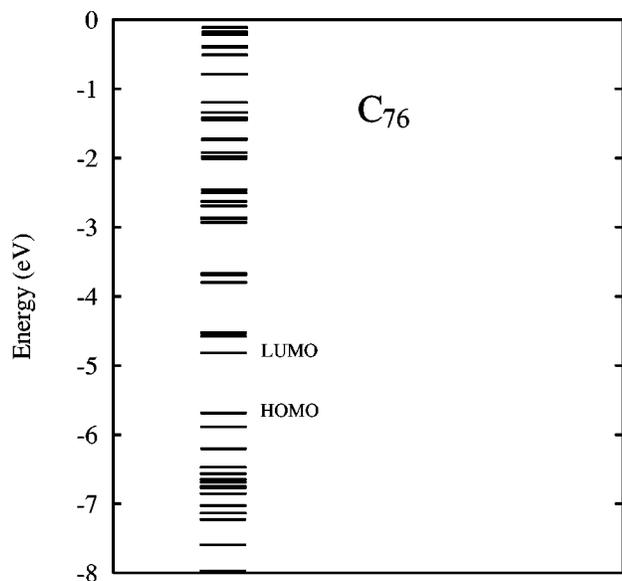
We first remark on the geometry of the molecule, which has a chiral D_2 symmetry [40]. The accepted geometry is depicted in Ref. [21]; it may be understood as follows. We start with C$_{60}$, in which all carbons are on pentagons. Group the pentagons into triangles and divide the fullerene in half keeping two adjacent triangles of pentagons intact in each half. The ''peel'' of six pentagons already has a chiral geometry dependent on the relative orientation of its two triangles of pentagons. The C$_{76}$ is constructed by adding 16 carbon atoms between the split halves of the C$_{60}$. The added carbon atoms lie entirely on hexagons which form a complete band around the fullerene. The inserted band has the geometry of an (8,2) chiral carbon nanotube. The result is then the chiral C$_{76}$. Our calculations are performed on a right-handed C$_{76}$, in the sense that the band of hexagons corresponds to a right-handed nanotube. This is the same convention as used in Ref. [40], their Fig. 3(d).
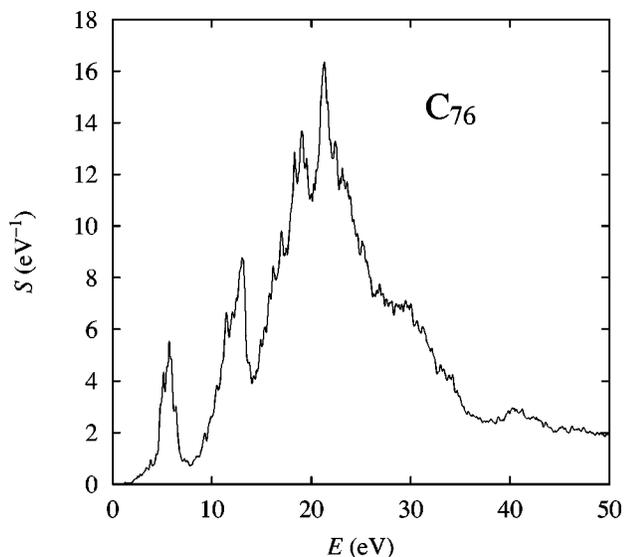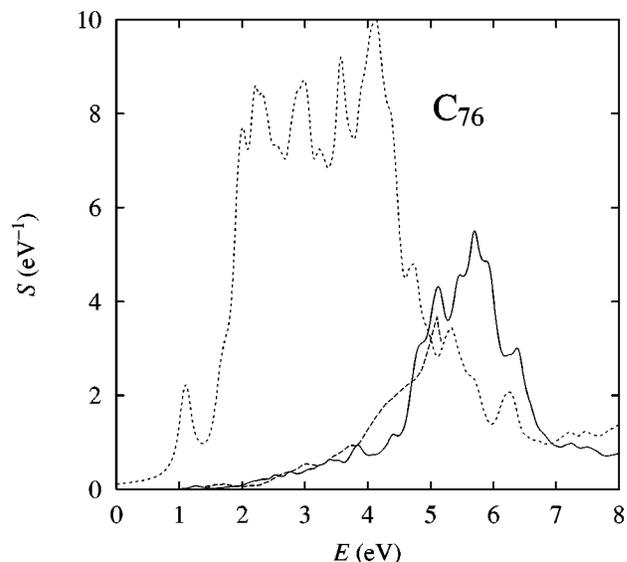
The C$_{76}$ has 152 occupied spatial orbitals. We show the orbitals near the Fermi level in Fig. 8. The HOMO-LUMO gap is only 0.9 eV, and there are many transitions in the optical region. In Fig. 9 we show the optical absorption strength function for the range 0–50 eV. Smoothing is made with the width of 0.2 eV in the Fourier transformation. A concentration of strength is apparent at 6 eV excitation; there is a similar peak in graphite and C$_{60}$ which is associated with $\pi - \pi^*$ transitions. The strong, broad peak centered near 20 eV is associated with $\sigma - \sigma^*$ transitions and is also present in C$_{60}$ [36]. The feature at 13 eV is not present in C$_{60}$, however. In the next figure, Fig. 10, we show a magnified view of the absorption at low energy. We also compare the TDLDA strength with the single-electron strength, smoothed also by convolution with a Breit-Wigner function of width $\Gamma = 0.2$ eV. The TDLDA has a strong influence on the strength distribution, decreasing the total strength in the low energy region and concentrating in the 6 eV peak. The experimental absorption strength [40] (with arbitrary normalization) is shown as the dashed line. It agrees with the TDLDA quite well.

We next examine the circular dichroism spectrum. Figure 11 shows the rotatory strength function between 0 and 50

FIG. 8. Static LDA orbitals in C_{76} near the Fermi level.

FIG. 10. Optical absorption spectrum of C_{76} in the range 0–8 eV. The dotted line is the single-electron strength, the solid line is the TDLDA, and the dashed line is the experiment [40].

eV. As in the case of methyloxirane, it is irregular without any large scale structures. Its integral is zero to an accuracy of 0.001 eV $Å^3$. The low energy region is shown in Fig. 12. Here one sees qualitative similarities between theory and experiment [21]. The theoretical sharp negative peak at 1.8 eV corresponds to an experimental peak at 2.2 eV. Shifting the higher spectra by that amount (0.6 eV), one sees a correspondence between the next positive and negative excursions. We note that a similar shift in the excitation energy was also seen in the optical absorption of C_{60} between the measurement and the TDLDA calculation [36]. As in the case of methyloxirane, the theoretical circular dichroism is somewhat too large; the experimental spectrum in Fig. 12 has been rescaled by a factor of 4.

Our theoretical optical rotatory power is plotted in Fig. 13. The situation here is different from the methyloxirane, in that rotatory power is large in a region where there are allowed transitions. The measured optical rotatory power,

$[\alpha]_D = -4000°$ at 2.1 eV [21] corresponding to $\beta = -7.3$ $Å^4$, is shown as the star. It does not agree with theory, but we should remember that the spectrum needs to be shifted by 0.6 eV to reproduce the circular dichroism. Adjusting the theoretical spectrum upward by that amount, we find that it is consistent in sign and order of magnitude with the measurement. Since the optical rotatory power in the region of allowed transitions changes rapidly as excitation energy, a measurement of the energy dependence would be very desirable, and would allow a more rigorous comparison with the theory.

V. CONCLUDING REMARKS

We have presented an application of the time-dependent local density approximation to the optical activities of chiral molecules. Our method is based on the uniform grid repre-

FIG. 9. Optical absorption spectrum of C_{76} in the range 0–50 eV.
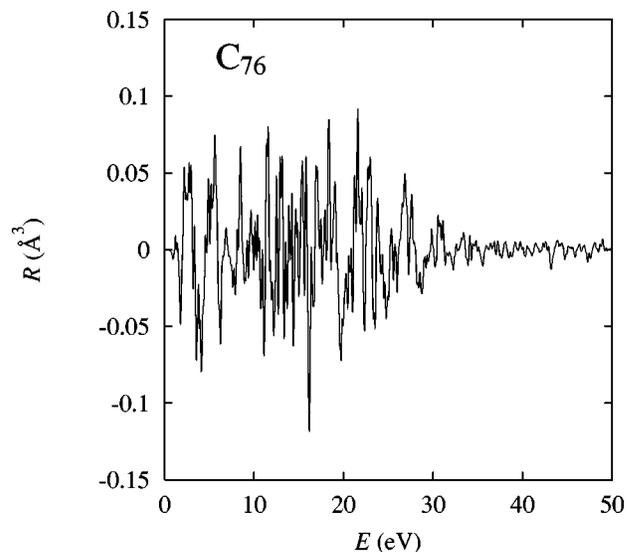
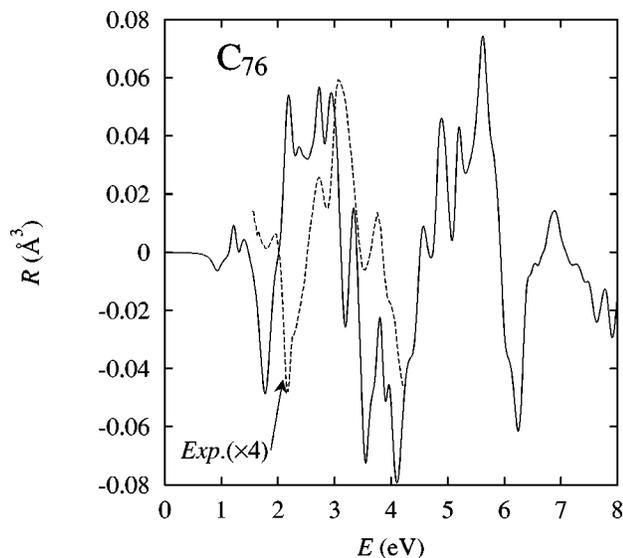FIG. 11. Circular dichroism spectrum of C_{76}.

FIG. 12. Circular dichroism spectrum of C_{76} comparing theory (solid line) and experiment (dashed line). The experimental data are from Ref. [21] and are with arbitrary normalization.

FIG. 13. Optical rotatory power of C_{76}, given as Re β in units of $\mathring{A}^4$. The star is the measured value from $[\alpha]_D$.

sentation of the wave function, real-time solution of the time-dependent Kohn-Sham equation, and the time-frequency Fourier transformation to obtain the response functions. In this way we can calculate the optical absorption, circular dichroism, and the optical rotatory power over a wide energy region, respecting sum rules and the Kramers-Kronig relation.

We applied our method to two molecules, methyloxirane and C_{76}. For the lowest two transitions of methyloxirane, the TDLDA reproduces the absorption and circular dichroism with an accuracy within a factor of 3. The qualitative feature of the circular dichroism spectrum of C_{76} is also reproduced rather well. However, the optical rotatory power is found to be a very sensitive function with strong cancellation. Even though we obtained the rotational strength of the full spectral
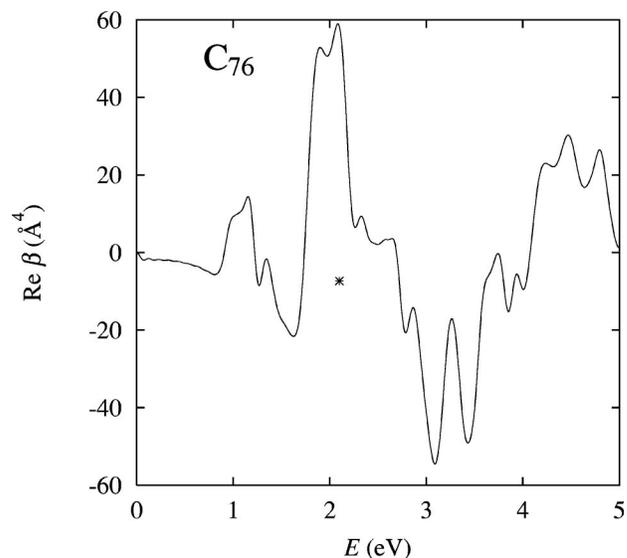
region, it is still difficult to make a quantitative prediction of optical rotatory power at low energies in our present approach.

[1] A. Zangwill and P. Soven, Phys. Rev. A **21**, 1561 (1980).
[2] Z.H. Levine and P. Soven, Phys. Rev. A **29**, 625 (1984).
[3] H. Zhong, Z.H. Levine, and J.W. Wilkins, Phys. Rev. A **43**, 4629 (1991).
[4] F. Alasia et al., J. Phys. B **27**, L643 (1994).
[5] M. Stener, P. Decleva, and A. Lisini, J. Phys. B **28**, 4973 (1995).
[6] C. Jamorski et al., J. Chem. Phys. **104**, 5134 (1996).
[7] A. Rubio et al., Phys. Rev. Lett. **77**, 247 (1996).
[8] K. Yabana and G.F. Bertsch, Phys. Rev. B **54**, 4484 (1996).
[9] K. Yabana and G.F. Bertsch, Z. Phys. D **42**, 219 (1997).
[10] C. Ullrich and E. Gross, Comments At. Mol. Phys. **33**, 211 (1997).
[11] M. Feyereisen et al., J. Chem. Phys. **96**, 2978 (1992).
[12] H. Koch et al., Chem. Phys. **172**, 12 (1993).
[13] Y. Luo et al., J. Phys. Chem. **98**, 7782 (1994).
[14] Y. Luo et al., Phys. Rev. B **51**, 14 949 (1995).
[15] M. Petersilka, U. Gossmann, and E. Gross, Phys. Rev. Lett. **76**, 1212 (1996).
[16] M. Carnell et al., Chem. Phys. Lett. **180**, 477 (1991).
[17] P.L. Polavarapu and D.K. Chakraborty, J. Am. Chem. Soc. **120**, 6160 (1998).
[18] M. Pericou-Cayere et al., Chem. Phys. **226**, 297 (1998).
[19] D. Cohen et al., J. Am. Chem. Soc. **105**, 1738 (1983).
[20] A. Breest et al., Mol. Phys. **82**, 539 (1994).
[21] J.M. Hawkins and A. Meyer, Science **260**, 1918 (1993).
[22] E.U. Condon, Rev. Mod. Phys. **9**, 432 (1937).
[23] A.E. Hansen and T.D. Bouman, Adv. Chem. Phys. **44**, 545 (1980).
[24] A. Moscowitz, Adv. Chem. Phys. **4**, 67 (1962).
[25] A.E. Hansen, Mol. Phys. **33**, 483 (1977).
[26] D. Caldwell, Mol. Phys. **33**, 495 (1977).
[27] I.B. Khriplovich and M.E. Pospelov, Phys. Lett. A **171**, 349 (1992).
[28] R.A. Harris, J. Chem. Phys. **50**, 3947 (1969).
[29] N. Troullier and J.L. Martins, Phys. Rev. B **43**, 1993 (1991).
[30] L. Kleinman and D. Bylander, Phys. Rev. Lett. **48**, 1425 (1982).

[31] D. Ceperley and B. Alder, Phys. Rev. Lett. **45**, 566 (1980).

[32] J. Perdew and A. Zunger, Phys. Rev. B **23**, 5048 (1981).

[33] R. van Leeuwen and E. J. Baerends, Phys. Rev. A **49**, 2421 (1994).

[34] J.P. Perdew, K. Burke, and M. Ernzerhof, Phys. Rev. Lett. **77**, 3865 (1996).

[35] J. Chelikowsky, N. Troullier, K. Wu, and Y. Saad, Phys. Rev. B **50**, 11 355 (1994).

[36] K. Yabana and G.F. Bertsch, e-print physics/980801.

[37] A. Rank, J. Am. Chem. Soc. **103**, 1023 (1981).

[38] M.E. Casida, C. Jamorski, K. Casida, and D.R. Salahub, J. Chem. Phys. **108**, 4439 (1998).

[39] G. Orlandi *et al.*, Chem. Phys. Lett. **224**, 113 (1994).

[40] R. Ettl, I. Chao, F. Diederich, and R.L. Whetten, Nature (London) **353**, 149 (1991).